Chromatographic Investigation of the Oxygen Exchange Reaction Between Carbon Monoxide and Carbon Dioxide

The theory of perturbation chromatography and isotopic tracers has been applied to the investigation of the oxygen exchange reaction between carbon monoxide and carbon dioxide in the presence of a copper-zinc oxide catalyst at 205°C and atmospheric pressure. By analyzing the retention times of carbon-14 monoxide and carbon-14 dioxide tracers in six binary carbon monoxide/carbon dioxide carrier gas streams, it has been possible to shed light on the mechanism of the exchange reaction. Two types of carbon monoxide adsorption and two types of carbon dioxide adsorption were identified. Based on a numerical simulation of the experimental data, it has been concluded that the exchange reaction proceeds via the dissociative adsorption of carbon dioxide. Furthermore, the surface oxygen species formed during the dissociative adsorption of carbon dioxide appears to be the active site for the exchange reaction.

W. D. SMITH
and
H. A. DEANS

Department of Chemical Engineering
Rice University
Houston, Texas 77001

SCOPE

The water gas shift reaction has been a reaction of considerable commercial importance for many years because of its value in hydrogen production. The first generation of water gas shift catalysts was composed of iron oxide. These catalysts were active only at high temperatures where hydrogen formation is thermodynamically limited. Second generation water gas shift catalysts consist of copper supported on zinc oxide or on a mixture of zinc oxide and alumina. These catalysts are active at much lower temperatures where hydrogen formation is favored.

This paper describes the results of a chromatographic study of a commercial copper-zinc oxide water gas shift catalyst. In particular, the method of interpreting the chromatographic data derived from the experiments represents an extension in the area of perturbation chromatography. The oxygen exchange reaction between carbon monoxide and carbon dioxide has been used as a test reaction to gain insight into the mechanism of oxygen transfer that occurs in the presence of this catalyst during the water gas shift reaction.

CONCLUSIONS AND SIGNIFICANCE

The method of interpreting the chromatographic data described in this paper has made it possible to extract more information from chromatographic data than ever before. Previously, analysis of tracer retention data relied on perturbation chromatography theory, which assumes that all adsorption and/or reaction processes occurring in the chromatographic column are at equilibrium. By varying the flow rate of carrier gas through the catalyst-packed column it was possible to obtain not only retention data which can be described by the equilibrium theories but also data falling in a transition region where one or more adsorption processes are neither negligible nor at equilibrium. In order to analyze the transition region data, the column was simulated numerically on a computer.

With this combined equilibrium-nonequilibrium method of analysis, a five-step adsorption-reaction mechanism has been developed to describe the exchange reaction over the entire range of the experimental data. The mechanism shows oxygen transfer to occur as a result of dissociative carbon dioxide adsorption. Furthermore, the appearance of the four adsorption isotherms developed in this study can be explained only if the active surface site for the exchange reaction is an oxygen site created by the dissociative adsorption of carbon dioxide. This mechanism represents a departure from the traditional view that the active site for the exchange reaction is a reduced (metallic) site.

In recent years chromatography has emerged as a useful tool for direct measurement of many physicochemical phenomena. By relating the moments of the eluted chromatographic peaks to the processes occurring within the column, investigators have been able to determine gas-liquid K-values (Stalkup and Kobayashi, 1963; Koonce et al., 1965), adsorption isotherms (Eberly, 1961; Helfferich and Peterson, 1963), intraparticle diffusion coefficients

W. D. Smith is with Exxon Production Research Company.

(Schneider and Smith, 1968), and axial dispersion coefficients (Taylor, 1953; Schneider and Smith, 1968). Recently, a generalized theory of direct chromatography (Deans et al., 1970), which includes nonlinear and coupling effects, was published.

The initial application of direct chromatography to gas-solid systems was in measuring adsorption isotherms, as reported by Eberly (1961). The use of isotopic tracers and multicomponent carrier gases was treated theoretically and experimentally by Helfferich and Peterson (1963), Stalkup and Deans (1963), Stalkup and Kobayashi (1963), and Koonce et al. (1965). Klinkenberg (1961) dealt theoretically with the case of adsorption with equilibrium chemical reaction in a chromatographic column. Later, Collins and Deans (1968) conducted a theoretical and experimental chromatographic investigation of chemically reactive gas-solid systems at equilibrium.

The purpose of this work was to extend direct, that is, equilibrium perturbation, chromatography using isotopic tracers to nonequilibrium chemically reactive systems. Musser (1965), in his study of carbon monoxide adsorption on a copper-zinc oxide catalyst, observed the presence of a nonequilibrium oxygen exchange reaction between carbon monoxide and carbon dioxide. In keeping with the original goal of the work and considering the importance of this reaction, it was decided to conduct a more detailed study of this system.

Copper supported on zinc oxide is used commercially as a water gas shift catalyst to take advantage of the more favorable water gas shift equilibrium at lower temperatures. The purpose of the zinc oxide, in addition to supporting the copper, is to inhibit thermal sintering of the finely dispersed copper. Uchida et al. (1968) concluded that the water gas shift activity of this type of catalyst can be related to the amount of copper present.

The oxygen exchange reaction between carbon monoxide and carbon dioxide,

$$CO + C^*O_2 \rightleftarrows C^*O + CO_2 \qquad (1)$$

where * denotes a detectable carbon isotope, represents a powerful investigative tool for studying the mechanism of the water gas shift reaction over this catalyst since oxygen exchange is the necessary step in the reaction,

$$CO + H_2O \rightleftarrows CO_2 + H_2 \qquad (2)$$

In this work the exchange reaction was initiated by injecting either a carbon-14 monoxide or a carbon-14 dioxide tracer sample into a binary carbon monoxide-carbon dioxide carrier gas flowing at equilibrium over activated catalyst. All experiments were carried out at 205°C and atmospheric pressure. By varying the carrier gas flow rate over a given column it was possible to vary residence time relative to adsorption and reaction half-lives, hence to alter the equilibrium approach of the isotopic exchange reaction.

EXPERIMENT

The experimental apparatus used in this work is depicted schematically in Figure 1. The feed cylinder was first filled with a carrier gas of accurately known composition. The cylinder was then connected to the system through a filter, a flow controller, and a metering valve. From this point the gas passed through a precolumn containing the same catalyst at the same temperature as the test column. The purpose of the precolumn was to adsorb any poisons which might be present in trace amounts in the carrier gas. The gas flowed from the precolumn to the reference side of a thermal conductivity cell and then a two position, six-way chromatographic sampling valve. The sample loop of the sampling valve was connected to a manifold through which tracers could be admitted. The gas stream then flowed from the sampling valve to the test column in the oven. The gas leaving the column then passed through the sample side of the thermal conductivity cell and on to the ionization chamber for carbon-14 tracer measurement. Finally the gas flowed through a soap bubble flow meter to a hood for dispersion to the atmosphere.

The thermal conductivity detector was used in this work primarily to ensure that the system was at equilibrium prior to sample injection. The ionization chamber was a flow-through cell with an internal volume of 3 cc. A 6 V potential was connected across the interior electrode and the outer wall. The current generated by the radioactive tracer in this cell was measured by a Cary Model 401 electrometer. The millivolt outputs of both detectors were recorded on a two channel Hewlett-Packard strip chart recorder.

Two stainless steel columns, both 0.64 cm in diameter, and 101.4 cm and 10.0 cm in length, respectively, were packed with Girdler G-66B copper-zinc oxide catalyst which had been ground and sieved to retain the 28/35 mesh fraction. The two lengths were necessary in order to achieve the desired range of residence time (0.25 to 300 sec.) without developing excessive pressure drop or uncontrollably low flow rates. The two columns were connected in series in such a way that the carrier gas flow could either be directed over the two columns in series or over only the short column simply by interchanging two connections outside the oven. By including both columns in the oven by this arrangement, only one catalyst activation was required, and any variables in this procedure were not reflected in the experimental results.

When two columns were connected in series, a capillary bypass was used to create a reference peak for comparison with the peak emerging from the column. The retention time of the tracer in the column could be determined from the difference between the first moments of the two peaks. It was not possible to use a capillary bypass with the short column, however, because poor resolution between the peaks resulted. The system was constructed in such a way, however, that a bypass peak could be recorded separately. A more detailed description of the column arrangement is given elsewhere (Smith, 1972).

As stated above, measurement of the retention time of the tracer in the column requires knowledge of the first moments of both bypass and column peaks. Although the first moment of a peak can be determined rigorously by graphical integration, a substitute method was used which proved to be rapid, reproducible, and adequately precise. A line was first drawn through the chromatogram at the half-height of the peak parallel to the baseline. The midpoint of the segment of this line falling within the peak was taken as the centroid. This method

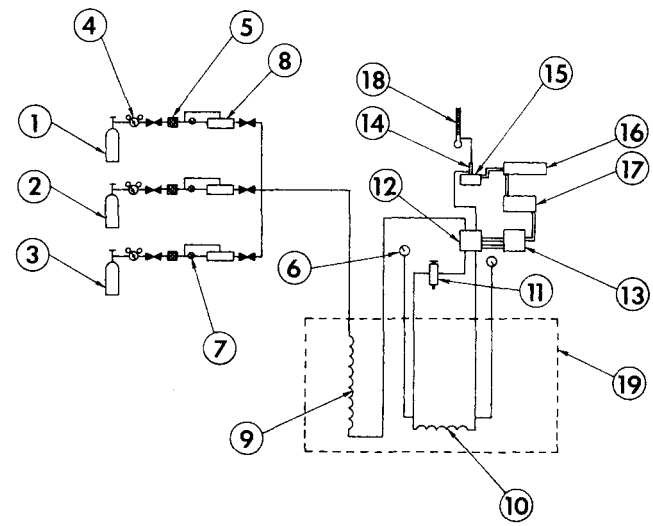

Fig. 1. Schematic flow diagram: 1. Hydrogen; 2. Helium; 3. Carrier gas; 4. Pressure regulator; 5. Filter; 6. Pressure gauge; 7. Metering valve; 8. Flow controller; 9. Precolumn; 10. Test column; 11. Sampling valve; 12. Thermal conductivity cell; 13. Bridge; 14. Ionization chamber; 15. Preamplifier; 16. Electrometer; 17. Recorder; 18. Soap bubble meter; and 19. Oven.

was checked in several instances against the graphical procedure, and the resulting values were found to be in close agreement. Furthermore, the short-cut method was insensitive to the uncertainty introduced by tailing.

Six equilibrium gas mixtures were used in this work. In addition to pure carbon monoxide and carbon dioxide, four mixtures of these two gases containing 94.7, 63.5, 27.6, and 6.5 vol. % carbon monoxide served as carrier gases. The mixtures were analyzed on a mass spectrometer. The purity of the gases used exceeded 99.5 vol. %, with the primary impurity in each gas being the other oxide.

The catalyst was activated by passing a mixture of hydrogen and helium over the catalyst (both columns in series) at atmospheric pressure and 205°C. The hydrogen concentration was maintained at 1 vol. % for the first 6 hours, at 2 vol. % for the second 6-hour period, and 5 vol. % for the final 6-hour period. Condensed water was observed in the exit lines, confirming that reduction of the catalyst was taking place. The system was purged of hydrogen and water by allowing helium to flow over the catalyst overnight.

The free gas volume of the system was determined by measuring the residence time of an argon sample in a helium carrier gas stream, assuming negligible argon adsorption at 205°C. This procedure was carried out for both columns connected in series and for the short column by itself. Following free volume calibration, flow of one of the premixed carrier gases was initiated over both columns.

When a steady thermal conductivity cell response indicated that the system was at equilibrium, data taking began. Appropriate flow, pressure, and temperature data were recorded, and then a sample of each tracer separately was injected into the carrier gas. The response of the ionization chamber to each sample was recorded on a strip chart recorder in the form of a typical chromatogram. The moments of these peaks were approximated by the method described previously.

This sampling and data taking procedure was repeated for a range of flow rates over both columns connected in series and also for the short column by itself. At no time was the column pressure drop allowed to exceed 20 N/m^2(3 lb./sq.in.).

This procedure resulted in a complete set of data for a particular carrier gas. The same procedure was then followed for each of the remaining carrier gases to generate the total set of experimental data.

EQUILIBRIUM THEORY

Collins and Deans (1968) developed the equilibrium theory for a chromatographic system characterized by an isotopic exchange reaction of the form

$$A + B^* \rightleftarrows A^* + B \tag{3}$$

where * denotes a nonnormal isotope. The results of Collins and Deans (1968) can be applied to the experimental system studied in this work if the following assumptions are made:

1. The column is isothermal and isobaric.
2. The carrier gas behaves ideally.
3. The column is one-dimensional.
4. Local equilibrium exists between the flowing phase and the stationary phase. Adsorption equilibrium can be expressed by the following equation:

$$\omega_i = \mu_i y_i \tag{4a}$$

where

$$\mu_i = \mu_i\,(T, P, y_A^s, y_B^s, \ldots) \tag{4b}$$

5. Dispersion effects are negligible.
6. The effect of the mass perturbation induced by sample injection can be neglected in the vicinity of the isotopic tracer.
7. Each isotopic tracer is chemically indistinguishable from its normal counterpart.
8. The equilibrium constant K^* of the isotopic exchange reaction in Equation (3) is equal to unity. The reaction equilibrium relationship is assumed to take the following form:

$$K^* = \frac{y_A^* y_B}{y_A y_B^*} \tag{5}$$

In the vicinity of the tracer, it can be shown that

$$y_A^*/y_B^* = y_A^s/y_B^s \tag{6}$$

In the limit of equilibrium adsorption and zero exchange reaction rate, the relative retention of each tracer is given by

$$G_A = \mu_A/\beta \tag{7a}$$

$$G_B = \mu_B/\beta \tag{7b}$$

where

$$\beta = \frac{m}{cV_g} \tag{7c}$$

G_i is an experimental quantity determined from the retention of the tracer according to the following equation:

$$G_i = \frac{1}{\beta}\left(\frac{t_{pi}}{t_r} - 1\right) \tag{8}$$

In the limit of equilibrium adsorption and equilibrium exchange reaction the relative retention is the same for each tracer and is given by

$$\beta G_e = y_A^s \mu_A + y_B^s \mu_B \tag{9}$$

NONEQUILIBRIUM ANALYSIS

In order to describe the system when the exchange reaction is neither negligible nor at equilibrium, it was necessary to simulate the column mathematically and obtain numerical solutions for the pulse response. The continuity equation for component i in the flowing phase can be written as

$$\frac{\partial y_i}{\partial t} + v\frac{\partial y_i}{\partial z} = D_e\frac{\partial^2 y_i}{\partial z^2} + R_i \tag{10}$$

Similarly, for the stationary phase, the material balance for surface component j is

$$\frac{\partial \omega_j}{\partial t} = R_j \tag{11}$$

Component i can participate in any of several types of adsorption according to the following equation for adsorption step k:

$$|\nu_{ik}|\ i\ (\text{gas}) \rightleftarrows |\nu_{jk}|\ j\ (\text{surface}) \tag{12}$$

The reaction shown in Equation (12) has a rate F_k, where

$$F_k = F_k\,(\{y_i\}, \{\omega_j\}, \text{rate constants}) \tag{13}$$

The source term in Equation (10) can then be expressed as follows:

$$R_i = \sum_{k=1}^{l} \nu_{ik} F_k \tag{14}$$

where l denotes the total number of local reactions in which component i participates.

The method of Deans and Lapidus (1960), in which column dispersion is modeled by representing the column by a series of perfectly mixed tanks, was used to simulate the data over the entire range of carrier gas residence times. The procedure first requires converting Equation (10) into stirred-tank form. When this is done, Equation (10) takes the following form for the nth tank:

$$\left[\frac{dy_i}{d\tau}\right]_n + (y_i)_n - \frac{V_t}{Q}(R_i)_n = (y_i)_{n-1} \tag{15}$$

The four-step mechanism shown in Equation (16) was first used in an attempt to explain the data but, as will be discussed later, was found to be inadequate.

$$\text{1. } CO + B \rightleftarrows \overset{CO}{\underset{|}{B}} \qquad (16a)$$

$$\text{2. } CO_2 + B \rightleftarrows \overset{CO_2}{\underset{|}{B}} \qquad (16b)$$

$$\text{3. } \overset{CO_2}{\underset{|}{B}} + B \rightleftarrows \overset{CO}{\underset{|}{B}} + \overset{O}{\underset{|}{B}} \qquad (16c)$$

$$\text{4. } CO_2 + C \rightleftarrows \overset{CO_2}{\underset{|}{C}} \qquad (16d)$$

The least complex mechanism found to satisfactorily explain the data is the five-step mechanism shown below.

$$\text{1. } CO + A \rightleftarrows \overset{CO}{\underset{|}{A}} \qquad (17a)$$

$$\text{2. } CO + \overset{O}{\underset{|}{B}} \rightleftarrows \overset{CO_2}{\underset{|}{B}} \qquad (17b)$$

$$\text{3. } CO_2 + \overset{O}{\underset{|}{B}} \rightleftarrows \overset{CO_3}{\underset{|}{B}} \qquad (17c)$$

$$\text{4. } \overset{CO_3}{\underset{|}{B}} + B \rightleftarrows \overset{CO_2}{\underset{|}{B}} + \overset{O}{\underset{|}{B}} \qquad (17d)$$

$$\text{5. } CO_2 + C \rightleftarrows \overset{CO_2}{\underset{|}{C}} \qquad (17e)$$

In this mechanism it can be seen that there are two adsorption steps (1 and 5) which are unrelated to the exchange reaction. The equilibrium relationships for these steps are assumed to be of the following form:

$$K_1 = \omega_{CO}^{A}/(y_{CO})\ (\omega_A) \qquad (18a)$$

$$K_2 = \omega_{CO}^{OB}/(y_{CO})\ (\omega_{OB}) \qquad (18b)$$

$$K_3 = \omega_{CO_2}^{OB}/(y_{CO_2})\ (\omega_{OB}) \qquad (18c)$$

$$K_4 = (\omega_{CO}^{OB})\ (\omega_{OB})/(\omega_{CO_2}^{OB})\ (\omega_B) \qquad (18d)$$

$$K_5 = (\omega_{CO_2}^{C})/(y_{CO_2})\ (\omega_C) \qquad (18e)$$

Collins and Deans (1968) showed that for a given carrier gas, the values of ω_A, ω_B, ω_C, and ω_{OB} are constant in the vicinity of the tracer. Consequently, Equations (18) can be rewritten in the following form:

$$\mu_{CO}^{A} = \omega_{CO}^{A}/y_{CO} \qquad (19a)$$

$$\mu_{CO}^{OB} = \omega_{CO}^{OB}/y_{CO} \qquad (19b)$$

$$\mu_{CO_2}^{OB} = \omega_{CO_2}^{OB}/y_{CO_2} \qquad (19c)$$

$$K' = \omega_{CO}^{OB}/\omega_{CO_2}^{OB} \qquad (19d)$$

$$\mu_{CO_2}^{C} = \omega_{CO_2}^{C}/y_{CO_2} \qquad (19e)$$

It should be pointed out that, although these adsorption relations are linear in form, it is not necessary for the adsorption isotherms to be linear. (The K_i in Equations (18) can also depend on concentration.) The rate expressions for the five steps in the mechanism are

$$F_1 = k_1\ (y_{CO} - \omega_{CO}^{A}/\mu_{CO}^{A}) \qquad (20a)$$

$$F_2 = k_2\ (y_{CO} - \omega_{CO}^{OB}/\mu_{CO}^{OB} \qquad (20b)$$

$$F_3 = k_3\ (y_{CO_2} - \omega_{CO_2}^{OB}/\mu_{CO_2}^{OB}) \qquad (20c)$$

$$F_4 = k_4\ (\omega_{CO_2}^{OB} - \omega_{CO}^{OB}/K') \qquad (20d)$$

$$F_5 = k_5\ (y_{CO_2} - \omega_{CO_2}^{C}/\mu_{CO_2}^{C}) \qquad (20e)$$

Again, these can be written in linear form because the perturbation is isotopic.

Equations (14) and (15) can then be combined to yield the following two equations for flowing phase carbon monoxide and carbon dioxide tracer concentrations in the nth tank:

$$\left[\frac{dy_{CO}}{d\tau}\right]_n + (y_{CO})_n + \left(\frac{V_t}{Q}\right)(F_1 + F_2) = (y_{CO})_{n-1} \qquad (21a)$$

$$\left[\frac{dy_{CO_2}}{d\tau}\right]_n + (y_{CO_2})_n + \left(\frac{V_t}{Q}\right)(F_3 + F_5) = (y_{CO_2})_{n-1} \qquad (21b)$$

For the surface species,

$$\frac{d\omega_{CO}^{A}}{d\tau} = \left(\frac{V_t}{Q}\right)(F_1) \qquad (22a)$$

$$\frac{d\omega_{CO}^{OB}}{d\tau} = (F_2 + F_4)\left(\frac{V_t}{Q}\right) \qquad (22b)$$

$$\frac{d\omega_{CO_2}^{OB}}{d\tau} = (F_3 - F_4)\left(\frac{V_t}{Q}\right) \qquad (22c)$$

$$\frac{d\omega_{CO_2}^{C}}{d\tau} = \left(\frac{V_t}{Q}\right)(F_5) \qquad (22d)$$

These equations were integrated numerically on an IBM 360 computer. Thirty tanks were used for all simulations. Simulation of one tracer sample took approximately 10 sec. of computer time although more time was required for samples with large retention times. Since the value of the exchange reaction equilibrium constant was assumed equal to one, K' is constrained and only four of the adsorption equilibrium functions shown in Equations (19) need to be specified.

The search procedure for the values of the four equilibrium constants was simplified by qualitatively observing that for most of the data steps 1 and 3 were near equilibrium at small carrier gas residence times while the effect of the other three steps was negligible. Therefore, these two rate constants were adjusted to maximum levels (to ensure equilibrium) while the values of the two equilibrium functions for a specific carrier gas were set according to the data and Equations (7). Therefore, only two

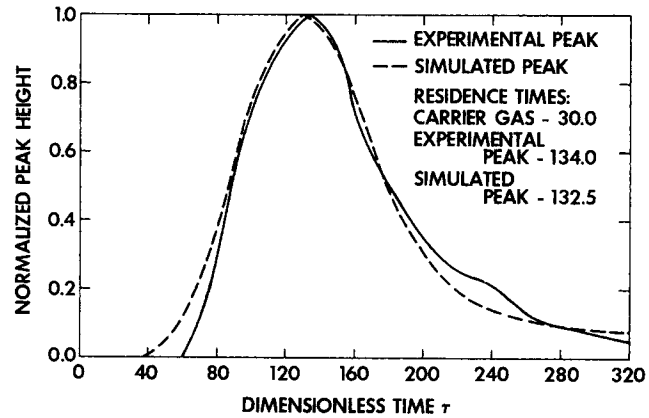

Fig. 2. Experimental and simulated peaks.

equilibrium functions and three rate constants remained to be adjusted in order to fit the data.

The retention time of the simulated peak was determined in the same manner as was described earlier for estimating the first moments of the experimental peaks. It is also possible to match the shape of the experimental peak by adding a post-column tank to account for the dispersion of the detection system. Although simulation of the retention data did not require that this be done, a few such simulations were made to demonstrate the reliability of the method. Figure 2 compares the shape of an experimental peak with a simulated one.

RESULTS

The final set of data is reported as the relative retention of each tracer over a range of carrier gas residence times of 0.2 to 300 sec. These data are plotted for each carrier gas in Figures 3 to 8. In plotting these data, the

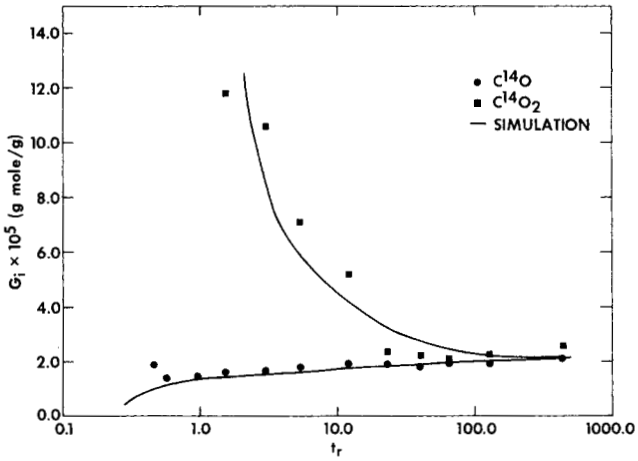

Fig. 3. G_i vs. t_r for 100% CO carrier gas.

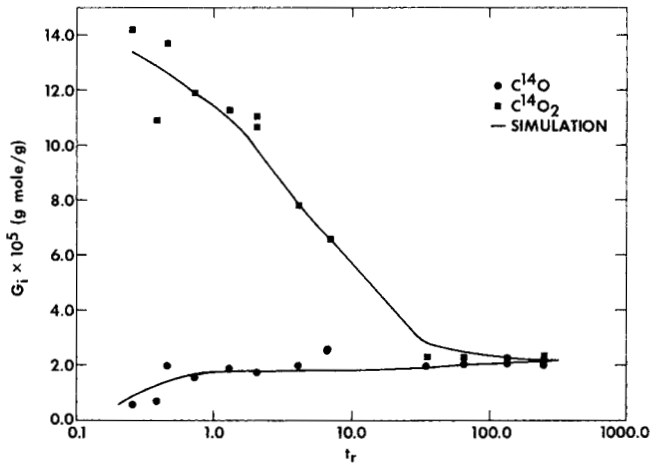

Fig. 4. G_i vs. t_r for 94.7% CO carrier gas.

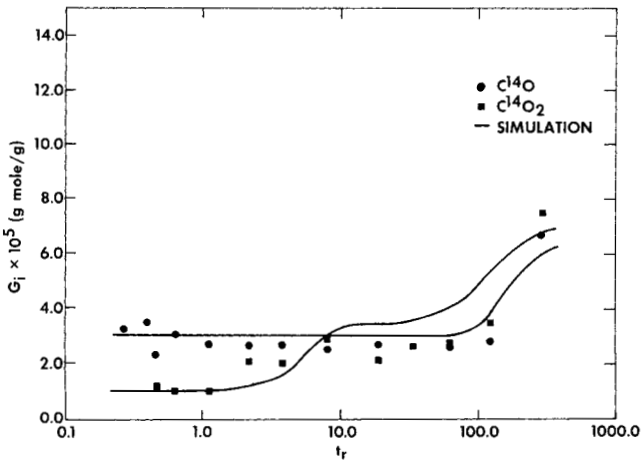

Fig. 5. G_i vs. t_r for 63.5% CO carrier gas.

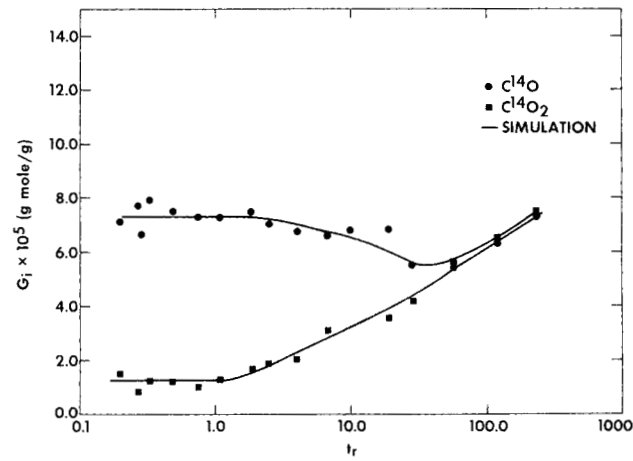

Fig. 6. G_i vs. t_r for 27.6% CO carrier gas.

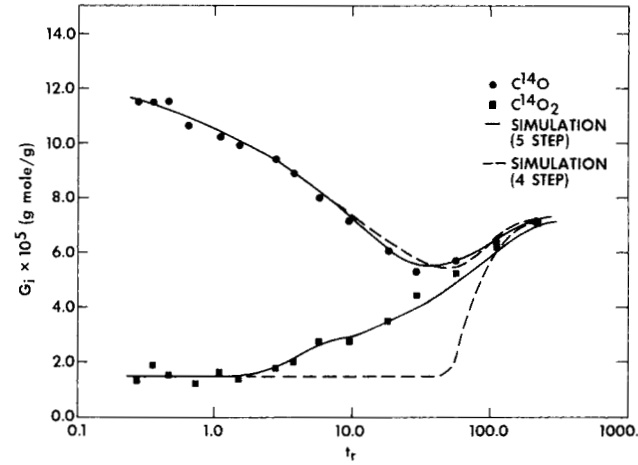

Fig. 7. G_i vs. t_r for 6.5% CO carrier gas.

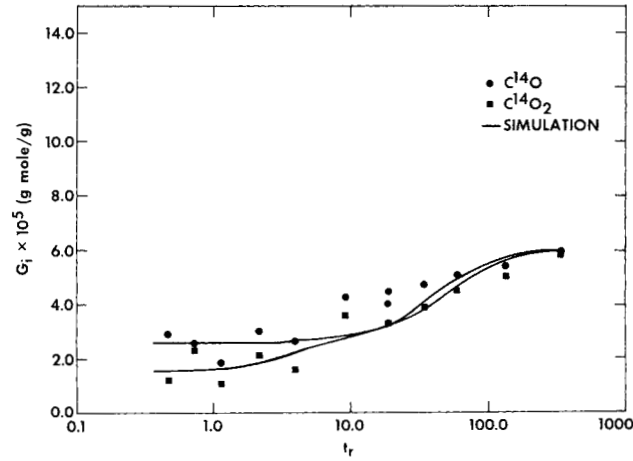

Fig. 8. G_i vs. t_r for 0% CO carrier gas.

carrier gas residence times for the long column were corrected to the short column basis to account for the difference in catalyst packing density for the two columns. In these figures the solid lines represent the results of best fits by numerical simulation, which will be discussed later.

Several qualitative features of the data are immediately obvious. For each carrier gas essentially the same retention time was observed for each tracer when the carrier gas residence time exceeded 250 sec. At small carrier gas residence times, each tracer has a unique response in every case except that of pure carbon dioxide carrier gas. The range of carrier gas residence times appears to include the limiting cases discussed earlier.

If the exchange reaction is negligibly slow and the adsorption processes are at equilibrium, the retention G_i for each tracer is given by Equations (7). Since this equation predicts no dependence on velocity (or carrier gas residence time), G_i should be independent of t_r. As the figures indicate, such a region is observed experimentally for carbon dioxide adsorption for the carrier gases containing 6.5, 27.4, and 63.5 mole % carbon monoxide. For carbon monoxide adsorption this region is clearly defined for the 27.4 mole % carbon monoxide carrier gas, and very nearly so for the 63.5 mole % carbon monoxide carrier gas.

For the data taken at large carrier gas residence times, Equation (9) relates G_i for either tracer to the carrier gas composition and adsorption equilibrium functions for the two components, carbon monoxide, and carbon dioxide. Again, the theory predicts G_i to be independent of the carrier gas residence time if both adsorption processes and the exchange reaction are at equilibrium. For carrier gases containing 100 and 94.7 mole % carbon monoxide, the large carrier gas residence time data appear to lie on a plateau which can be defined by Equation (9). For the carrier gas containing 63.5 mole % carbon monoxide, the data falling between carrier gas residence times of from 10 to 80 sec. also appear to define such a plateau. But when the carrier gas residence time exceeds 80 sec., G_i begins to increase for both tracers. This indicates the presence of an additional slow adsorption step which is not involved in the exchange reaction.

This slow step can be tentatively identified as a carbon dioxide adsorption step from the data of Figure 5. At larger values of t_r, the value of G_i for the carbon dioxide tracer slightly exceeds the value of G_i for the carbon monoxide tracer. This is in contrast to the fact that at low carrier gas residence times the G_i value for the carbon dioxide tracer is smaller than for the carbon monoxide tracer. This characteristic of the data was also predicted in the simulation.

For the carrier gases containing 100 and 94.7 mole % carbon monoxide, it can be argued that this adsorption step would have been observed if it had been possible to collect data at higher carrier gas residence times. It is also possible that the sites for the slow step are not present in sufficient number in carrier gases containing predominantly carbon monoxide.

At sufficiently large carrier gas residence times G_i would be expected to level off at a new plateau, once again according to Equation (9). In any case, two types of adsorption are apparent for carbon dioxide. A feature of direct chromatographic studies which this work serves to emphasize is that although various types of adsorption by the same component cannot be distinguished from each other if they are all at equilibrium, they can be observed separately if they differ in rate.

From the qualitative analysis of the data to this point, the following can be concluded:

1. There is at least one type of carbon monoxide adsorption which is relatively rapid.
2. There are at least two different types of carbon dioxide adsorption, one rapid and one slow.
3. The exchange reaction occurs at a rate which is slower than the rapid adsorption rates of carbon monoxide and carbon dioxide.
4. The second type of carbon dioxide adsorption is a slower process than the exchange reaction itself and is not necessary for the exchange reaction to occur.

Based on these observations the mechanism shown in Equations (16) was used in an attempt to simulate the data. The broken line in Figure 7 represents the best fit obtained using this mechanism for the carrier gas containing 6.5 mole % carbon monoxide. The disagreement between the experimental data and the results of the simulation indicate that the four-step mechanism is inadequate.

In order to satisfactorily explain the data, the four-step mechanism was expanded to the five-step mechanism shown in Equations (17) by the addition of a second carbon monoxide adsorption step. In this mechanism step 1 now corresponds to the rapid carbon monoxide adsorption. For the purpose of simulating the data shown in Figures 3 to 8 it is not necessary to make any assumptions regarding the nature of the active sites. Evidence suggesting that the active sites (O-B) contain oxygen will be introduced later.

The results of the five-step simulations are represented by the solid lines in Figures 3 to 8. In simulating the data in Figure 8, it was assumed that the carrier gas contained 0.5 vol. % carbon monoxide because of the purity of the carbon dioxide. This mechanism explains the data reasonably well. From the numerical simulations four adsorption equilibrium functions were determined for each carrier gas composition. This allowed calculation of the surface coverages for each type of adsorption according to Equation (4a). The resulting isotherms are plotted in Figures 9 to 12. The isotherms in Figures 9 and 10 for the rapid carbon monoxide adsorption (type A) and the

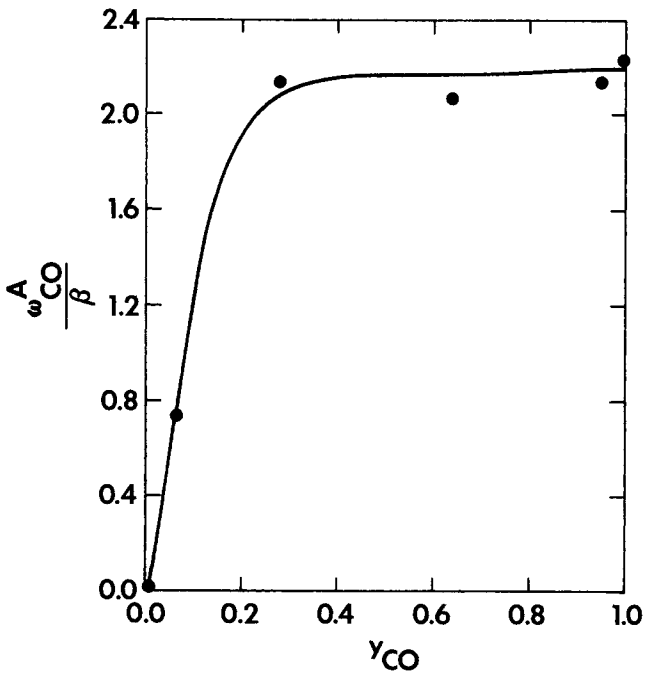

Fig. 9. Type A carbon monoxide adsorption isotherm.

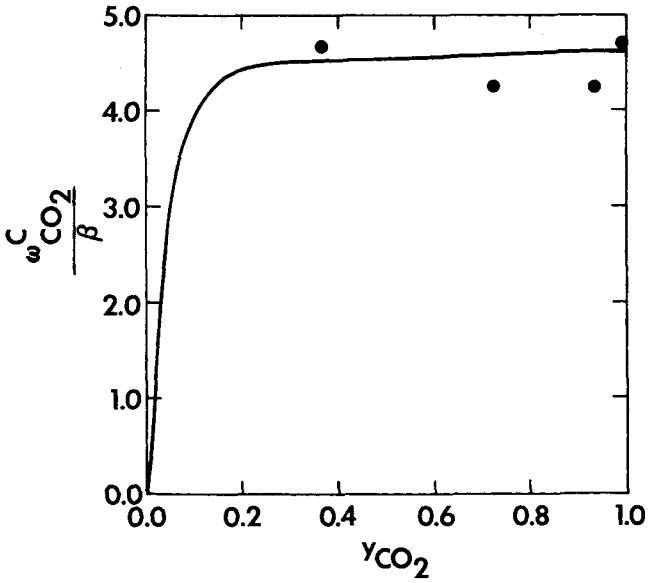

Fig. 10. Type C carbon dioxide adsorption isotherm.

slow carbon dioxide adsorption (type C), respectively, are normal in appearance. The type B carbon dioxide and carbon monoxide adsorption isotherms, Figures 11 and 12, respectively, are unusual. The concave appearance of the carbon dioxide isotherm can best be explained if the number of sites available for this type of carbon dioxide adsorption increases as the carbon dioxide content of the carrier gas increases. This also explains the shape of the carbon monoxide isotherm in Figure 12, if the same sites are involved. Another significant characteristic of the isotherm in Figure 12 is that the intercept for pure carbon monoxide is nonzero, that is, the concentration of the carbon dioxide related sites does not go to zero as the carbon dioxide concentration of the carrier gas does.

These isotherms indicate that the exchange reaction occurs via dissociative carbon dioxide adsorption [represented by Equations (17c) and (17d)], not intermolecular oxygen exchange between adjacently-adsorbed molecules. Dissociative carbon dioxide adsorption results in creating a surface oxygen species. The amount of surface oxygen can be expected to increase as the carbon dioxide content of the carrier gas increases. Consequently, the accumulation or depletion of oxygen on the catalyst surface follows the same pattern as the available adsorption sites in the explanation of the type B carbon monoxide and carbon dioxide isotherms. It is therefore consistent with dissociative carbon dioxide adsorption and the nature of the isotherms in Figures 11 and 12 if the oxygen remaining on the surface as a result of dissociative carbon dioxide adsorption serves as the active site for both carbon dioxide and carbon monoxide adsorption leading to the exchange reaction.

This interpretation implies that as the composition of the carrier gas approaches pure carbon monoxide, the amount of oxygen left on the surface to serve as carbon monoxide adsorption sites should approach zero. The nonzero intercept of the carbon monoxide isotherm in Figure 12 can be explained if it is assumed that two surface oxygen sites must be adjacent to one another for the reaction in Equation (17d) to occur. As the carbon monoxide content of the carrier gas increases, a point is reached at which all the remaining surface oxygen is surrounded by oxygen-free sites. These residual oxygen atoms cannot be removed according to Equation (17d). This explanation assumes that these adsorbed oxygen species have no surface mobility. This is reasonable at 205°C.

The question arises as to whether or not carbon monoxide or carbon dioxide adsorb on the unoxygenated B-sites. If carbon dioxide were to adsorb appreciably on these sites, the concave nature of the isotherm in Figure 11 would be destroyed. Carbon monoxide adsorption on the reduced sites cannot be ruled out completely. In fact, such adsorption could contribute partially to the nonzero intercept in Figure 12. But if this type of adsorption does occur, it necessarily occurs at very nearly the same rate as carbon monoxide adsorption on the oxygenated sites. Otherwise, this process would have become evident during the simulation of the data.

It has been reported in the literature (Uchida et al., 1968; Young and Clark, 1973) that water gas shift activity over supported copper catalysts is related to the amount of copper present. Stroeva et al. (1959) observed the oxygen exchange reaction between the carbon oxides in the presence of a copper film. Winter (1958) noted that this reaction has been observed to proceed quite

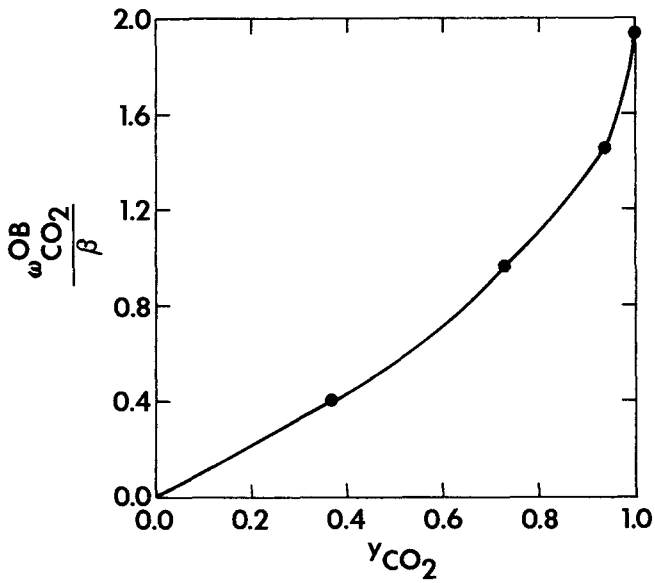

Fig. 11. Type B carbon dioxide adsorption isotherm.

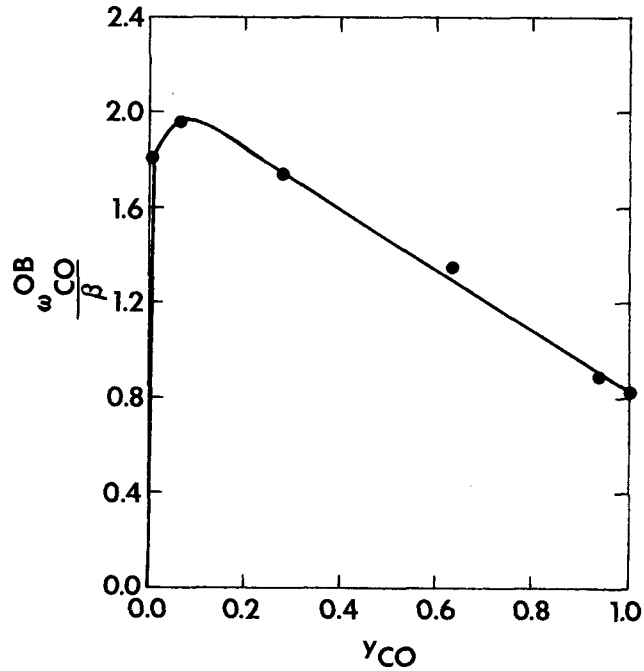

Fig. 12. Type B carbon monoxide adsorption isotherm.

slowly over zinc oxide. This evidence supports the belief that the exchange reaction is associated primarily with the copper. The B-sites in Equation (17) would correspond to reduced copper atoms. The oxygenated B-sites could correspond to a surface form of copper oxide. The exchange reaction might then proceed as follows:

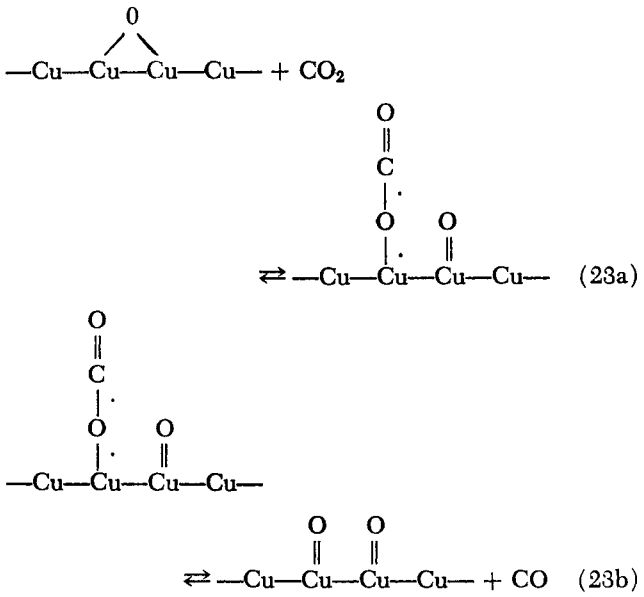

(23a)

(23b)

Perhaps the structure of the surface oxide could be more akin to that in Equation (24).

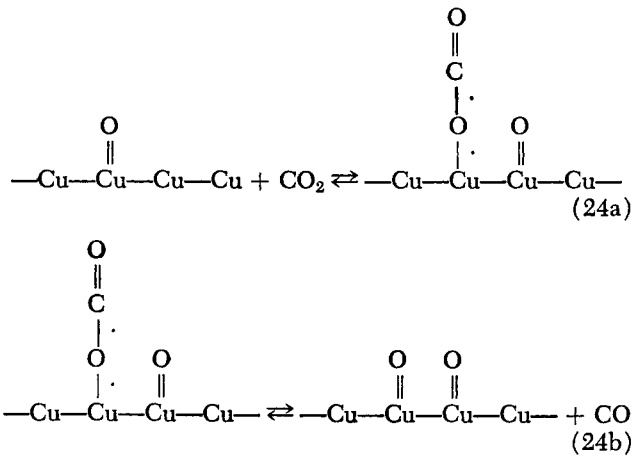

(24a)

(24b)

The question of the observed negligible carbon monoxide adsorption on the unoxygenated site was discussed earlier. Although carbon monoxide is known to adsorb strongly on metals, most of these studies have been conducted at low temperatures. Carbon monoxide adsorption on copper may not be appreciable at 205°C.

The character of the carbon monoxide and carbon dioxide adsorption sites in Equations (17a) and (17e), respectively, is not clear. However, since these types of adsorption processes appear unrelated to the exchange reaction, these sites could very well be associated with the zinc oxide support.

CONCLUSIONS

The application of the theory of perturbation chromatography and the use of isotopic tracers has been extended further to the investigation of chemical reaction in the presence of a solid catalyst. Interpretation of the experimental data has resulted in several conclusions with respect to the adsorption of carbon monoxide and carbon dioxide on this catalyst.

It has been shown that nothing less than a five-step mechanism can be used to explain the data. This mechanism includes two types of carbon monoxide adsorption and two types of carbon dioxide adsorption. In both cases these types of adsorption can be differentiated by rate. It has also been shown that the exchange reaction occurs via dissociative carbon dioxide absorption in preference to intermolecular oxygen transfer between adjacently-adsorbed carbon monoxide and carbon dioxide.

Additional evidence indicates that the active sites for both carbon monoxide and carbon dioxide adsorption leading to the exchange reaction are oxygen sites created by the dissociative adsorption of carbon dioxide. Furthermore, the literature suggests that the copper is involved in the exchange reaction.

ACKNOWLEDGMENTS

The authors would like to express their gratitude to Dr. C. R. Hocott and the Esso Production Research Company for providing the computer time. The authors would also like to express their appreciation to the National Science Foundation for financial support.

NOTATION

c = total gas phase concentration, moles/cc
D_e = effective axial dispersion coefficient, cm^2/s
F_k = rate of local reaction k, s^{-1}
G_i = relative retention time of tracer i, mole/g
k_k = local reaction rate constant for step k, s^{-1}
K_k = equilibrium constant for local reaction k
K^* = equilibrium constant for exchange reaction
K' = surface reaction equilibrium constant
m = mass of catalyst, g
P = pressure, N/m^2
Q = column flow rate, cc/s
R_i = source of component i, s^{-1}
t = time, s
t_{pi} = residence time of tracer i in column, s
t_r = carrier gas residence time in column, s
T = temperature, °C
v = velocity, cm/s
V_g = column free gas volume, cc
V_t = volume of single tank, cc
y_i = mole fraction of component i in carrier gas
y_i^s = mole fraction of component i at steady state
y_i^* = mole fraction of tracer component i
z = flowing phase direction, cm

Greek Letters

μ_i = adsorption equilibrium function for component i
μ_i^p = adsorption equilibrium function for component i on site p
ν_{ik} = stoichiometric coefficient of component i in local reaction k
τ = dimensionless time
ω_i = stationary phase concentration of component i, moles i/mole flowing phase
ω_i^p = stationary phase concentration of component i on site p, moles i/mole flowing phase

LITERATURE CITED

Collins, C. G., and H. A. Deans, "Direct Chromatographic Equilibrium Studies in Chemically Reactive Gas-Solid Systems," *AIChE J.*, 14, 25 (1968).

Deans, H. A., F. J. M. Horn, and G. Klauser, "Perturbation Chromatography in Chemically Reactive Systems," *ibid.*, **16**, 426 (1970).

Deans, H. A., and L. Lapidus, "A Computational Model for Predicting and Correlating the Behavior of Fixed Bed Reac-

tors: I. Derivation of Model for Nonreactive Systems," *ibid.*, **6**, 656 (1960).
Eberly, P. E., Jr., "High Temperature Adsorption Studies on 13X Molecular Sieve and Other Porous Solids by Pulse Flow Techniques," *J. Phys. Chem.*, **65**, 68 (1961).
Helfferich, F., and D. L. Peterson, "Accurate Chromatographic Method for Sorption Isotherms and Phase Equilibria," *Science*, **142**, 661 (1963).
Klinkenberg, A., "Chromatography of Substances Undergoing Slow Reversible Chemical Reactions," *Chem. Eng. Sci.*, **15**, 255 (1961).
Koonce, K. T., H. A. Deans, and R. Kobayashi, "Generalization of Gas-Liquid Partition Chromatography to Study High Pressure Vapor-Liquid Equilibria of Multicomponent Systems," *AIChE J.*, **11**, 259 (1965).
Musser, G. S., "A Perturbation Chromatographic Investigation of Chemisorption and Chemical Reaction on a Solid Catalyst," Ph.D. thesis, Rice University, Texas (1965).
Schneider, P., and J. M. Smith, "Adsorption Rate Constants From Chromatography," *AIChE J.*, **14**, 762 (1968).
Smith, W. D., "A Chromatographic Study of the Oxygen Exchange Reaction Between Carbon Monoxide and Carbon Dioxide Over a Cu-ZnO Catalyst," Ph.D. thesis, Rice University, Texas (1972).
Stalkup, F. I., and H. A. Deans, "Perturbation Velocities in Gas-Liquid Partition Chromatographic Columns," *AIChE J.*, **9**, 106 (1963).
Stalkup, F. I., and R. Kobayashi, "Vapor-Liquid Equilibrium Constants at Infinite Dilution Determined by Gas Chromatography: Ethane, Propane, and N-Butane in the Methane-Decane System," *J. Chem. Eng. Data*, **8**, 564 (1963).
Stroeva, S. S., N. V. Kulkova, and M. E. Temkin, "The Isotopic Exchange Reaction Between CO and C^*O_2 on Various Surfaces," *Doklady Akad. Nauk. S.S.S.R.*, **124**, 628 (1959).
Taylor, G., "Dispersion of Soluble Matter in Solvent Flowing Slowly Through a Tube," *Proc. Roy. Soc.*, **A219**, 186 (1953).
Uchida, H., M. Oba, N. Isogai, and T. Hasegawa, "The Zinc Oxide-Copper Catalyst for Carbon Monoxide-Shift Conversion. II. The Catalytic Activity and the Catalyst Structures," *Bull. Chem. Soc. Japan*, **41**, 479 (1968).
Winter, E. R. S., "The Reactivity of Oxide Surfaces," *Advances in Catalysis*, **10**, 196 (1958).
Young, P. W., and C. B. Clark, "Why Shift Catalysts Deactivate," *Chem. Eng. Prog.*, **69**(5), 69 (1973).

Manuscript received October 24, 1973; revision received and accepted April 19, 1974.

Gas Absorption by Non-Newtonian Fluids in Agitated Vessels

Carbon dioxide was absorbed by aqueous Carbopol solutions in a turbine-agitated vessel for the cases of absorption across an unbroken interface and absorption with the gas bubbling through the liquid. The rheological behavior of the solutions was described by the non-Newtonian power law model with flow behavior indices varying from 0.92 to 0.59. An effective viscosity technique which had previously been developed to correlate agitated vessel rates of viscous dissipation and heat transfer with power law pseudoplastic fluids was used to correlate the data.

JEROME F. PEREZ
and
ORVILLE C. SANDALL

Department of Chemical and Nuclear Engineering
University of California
Santa Barbara, California 93106

SCOPE

Gas absorption in mechanically agitated vessels is used in a variety of industrial applications and has been studied extensively for Newtonian liquids in various types of apparatus. In the work described here, gas absorption by non-Newtonian pseudoplastic liquids in agitated vessels is studied. The particular system chosen for the study is carbon dioxide absorption in various aqueous Carbopol (carboxy polymethylene) solutions. The rheological behavior of these solutions is well described by the Ostwald-de Waele power law model with the flow behavior index varying between 0.92 and 0.59. The agitated vessel geometry corresponded to the Standard Tank Configuration (Holland and Chapman, 1966); the impeller used was a six flat blade turbine.

Two methods of gas-liquid contact were studied. In the first method, the gas was introduced into the absorption vessel above the gas-liquid interface. This technique provided an unbroken gas-liquid interface of known area. In the second case, mass transfer occurred in a gas-liquid dispersion caused by introducing the gas through a sparge tube located in the liquid directly below the impeller.

CONCLUSIONS AND SIGNIFICANCE

The gas absorption data were successfully correlated using an effective viscosity technique which previously had been developed to correlate rates of viscous dissipation and heat transfer for pseudoplastic liquids. The effective viscosity is defined as the ratio of the shear stress corresponding to an average shear rate existing in the agitated vessel to this average shear rate. The average shear rate is empirically found to be proportional to the impeller speed. For the turbine impeller used in the experiments the effective viscosity is given by Equation (8).